

The Distance, Mass, and Radius of the Neutron Star in 4U 1608–52

Tolga Güver¹, Feryal Özel¹, Antonio Cabrera-Lavers^{2,3} and Patricia Wroblewski¹

¹ *University of Arizona, Department of Astronomy, 933 N. Cherry Ave., Tucson, AZ*

² *Instituto de Astrofísica de Canarias, E-38205 La Laguna, Tenerife, Spain*

³ *GTC Project Office, E-38205 La Laguna, Tenerife, Spain*

ABSTRACT

Low mass X-ray binaries that show thermonuclear bursts are ideal sources for constraining the equation of state of neutron star matter. The lack of independent distance measurements for most of these sources, however, prevents a systematic exploration of the masses and radii of the neutron stars, hence limiting the equation of state studies. We present here a measurement of the distance to the low mass X-ray binary 4U 1608–52 that is based on the study of the interstellar extinction towards the source. We first model the individual absorption edges of the elements Ne and Mg in the high resolution X-ray spectrum obtained with XMM-Newton. We then combine this information with a measurement of the run of reddening with distance using red clump stars and determine a minimum distance to the source of 3.9 kpc, with a most probable value of 5.8 kpc. Finally, we analyze time-resolved X-ray spectra of Type-I X-ray bursts observed from this source to measure the mass and the radius of the neutron star. We find a mass of $M = 1.74 \pm 0.14 M_{\odot}$ and a radius of $R = 9.3 \pm 1.0$ km, respectively. This mass and radius can be achieved by several multi-nucleon equations of state.

Subject headings: stars: neutron - X-ray: individual (4U 1608–52)

1. Introduction

The potential of utilizing low mass X-ray binaries (LMXBs) that show thermonuclear X-ray bursts to measure the masses and radii of their neutron stars has long been recognized (see, e.g., van Paradijs 1978, 1979; Lewin, van Paradijs, & Taam 1993). During these short lived flashes, bright thermal emission from the surface of the neutron star is observed, allowing, in principle, a measurement of the stellar radius or its surface gravity. Indeed, a

number of methods that involve the luminosity, surface redshift, or flux oscillations during these bursts have been proposed and used to measure or constrain the masses and radii of neutron stars in LMXBs (for a recent review, see Lattimer & Prakash 2007). Here, we focus on the time resolved X-ray spectroscopy of thermonuclear X-ray bursts observed from 4U 1608–52 in order to measure both the mass and the radius of its neutron star.

In a subset of thermonuclear bursts called photospheric radius expansion (PRE) bursts, the source flux reaches a peak that is thought to correspond to the local Eddington flux on the stellar surface, which is related to the mass and the radius of the neutron star. A second spectroscopic quantity that can be used to infer the mass and the radius of the neutron star is observed during the cooling tails of thermonuclear bursts. During this cooling phase, the measured apparent area of the emitting region remains constant while both the flux and the color temperature decrease. It has been shown that the observed surface areas remain constant between different bursts of the same source (Galloway et al. 2008a), indicating that the emission arises from a reproducible area on the stellar surface, likely corresponding to the entire neutron star surface. In addition to these two spectroscopic quantities, determining both the neutron star mass and its radius requires an independent distance or gravitational redshift measurement (see, e.g., Özel 2006; Özel, Güver, & Psaltis 2009; for a review of earlier results, see Lewin et al. 1993).

Apart from sources in globular clusters, independent measurements of distances to LMXBs have been a long-standing challenge (see, e.g., van Paradijs & White 1995). With the advances in high resolution X-ray grating spectroscopy, it is now possible to determine the X-ray absorption towards LMXBs with enough precision to allow studies of the properties of interstellar matter (ISM) towards these sources (see, e.g., Juett, Schulz, & Chakrabarty 2004; Juett et al. 2006; Wroblewski, Güver, & Özel 2008). Extinction measurement can in principle allow for a distance measurement if combined with a good standard candle within the field of view to an X-ray binary. Red clump stars have shown to be such standard candles (Paczynski & Stanek 1998; López-Corredoira et al. 2002). They are core helium-burning giants that form a well-defined concentration of stars in a color-magnitude diagram. Because their luminosities are largely independent of the total stellar mass and their infrared colors are insensitive to metallicity, they can be used to measure the run of reddening with distance. Finding the distances to LMXBs, then, involves a comparison of the extinction measurement of the X-ray source to that of red clump stars in the same field of view. A very similar technique has already been successfully applied to anomalous X-ray pulsars by Durant & van Kerkwijk (2006a, 2006b).

In this study, we measure the distance to the low mass X-ray binary 4U 1608–52 using the red clump method in order to ultimately determine the mass and the radius of its neutron

star. In detail, we *(i)* use high resolution X-ray spectroscopy to measure the column density in metals by modeling the absorption edges of Mg and Ne; *(ii)* use the interstellar abundance model of Wilms, Allen, & McCray (2000) to determine the amount of equivalent hydrogen column density towards the source; *(iii)* use observed relations between $N_{\text{H}} - A_V$ (Görenstein 1975; Güver & Özel 2009) and $A_V - A_K$ (Cardelli, Clayton, & Mathis 1989) to convert to infrared extinction A_K ; *(iv)* create a near-IR color-magnitude diagram of the field towards the X-ray binary to determine the run of reddening with distance using red clump stars; and *(v)* compare the infrared extinction A_K to the source with this run of reddening with distance to measure the distance to the X-ray binary. Finally, we *(vi)* fit X-ray burst spectra to measure the Eddington flux and apparent area of 4U 1608–52 and combine these with the distance measurement to derive the mass and radius of the neutron star.

4U 1608–52 is a transient X-ray burster that was first detected by the two Vela-5 satellites (Belian, Conner, & Evans 1976). Subsequent Uhuru observations confirmed the connection between the bursting and the persistent source (Tananbaum et al. 1976). A more precise X-ray position, obtained with HEAO-1, permitted the identification of the optical counterpart, QX Normae, with a $I=18.2$ magnitude (Grindlay & Liller 1978). Wachter et al. (2002) identified a modulation in the optical light curve of the source with a period of 0.537 days, which they attributed to the orbital period. 4U 1608–52 has also been observed during several outbursts with the Rossi X-ray Timing Explorer (RXTE). 31 Type-I X-ray bursts were identified, out of which 12 were categorized as PRE bursts. During several PRE bursts, burst oscillations have been detected with a frequency of 619 Hz, making this source one of the most rapidly rotating accreting neutron-stars (Galloway et al. 2008a).

In §2, we measure the galactic hydrogen column density towards the source using absorption edges of individual elements. We measure the distance to the source in §3, using its hydrogen column density in conjunction with the red clump stars. In §4, we present results of the time resolved spectral modeling of Type-I X-ray bursts. In §5, we use the distance and the results from the burst modeling to determine the mass and the radius of the neutron star. Finally, we discuss our results and its implications in §6.

2. The Hydrogen Column Density Towards 4U 1608–52

In this study, we make use of the hydrogen column density towards 4U 1608–52 in two ways: *(i)* to measure the distance to the X-ray binary and *(ii)* to model the time resolved X-ray spectra obtained with the RXTE. We, therefore, begin our analysis with a measurement of the galactic X-ray absorption from high resolution X-ray spectra.

We determine the amount of the interstellar X-ray absorption by modeling the individual absorption edges of the elements Ne and Mg in the X-ray grating spectra of the source obtained with the Reflection Grating Spectrometer (RGS) onboard XMM-Newton. This approach does not rely on an assumption of the intrinsic broadband X-ray spectrum of the source and is similar to the method previously applied to a number of low-mass X-ray binaries by Juett et al. (2004, 2006) and Wroblewski et al. (2008) and to anomalous X-ray pulsars by Durant & van Kerkwijk (2006a).

4U 1608–52 has been observed 4 times with XMM-Newton. A list of these observations together with the exposure time are given in Table 1. The source was in a quiescent state during three of the four observations, rendering very low counts. In addition, due to the high energy particle background during the last observation (Obs ID : 0149180201), only 5 ks of this observation were usable. Even though 4U 1608–52 was in an outburst during this observation, the short exposure time as well as the intrinsic spectrum of the binary prevented us from measuring the optical depths of the Si, O, and Fe edges. Future grating observations of this source during an outburst phase would also enable a measurement of these edges.

We extracted RGS spectra with the latest calibration files available (as of March 23 2009) and used the *rgsproc* tool within SAS v.7.1.0. By default, the binning of X-ray grating spectra oversamples the instrumental resolution of the RGS detectors. For this reason, we rebinned the resulting spectra by a factor of 5 to match the wavelength resolution of the detector (0.04 Å). The resulting X-ray spectrum had approximately 300 counts at the Mg edge and 40 counts at the Ne edge per spectral bin. To analyze the spectra, we used XSPEC v12 (Arnaud et al. 1996).

We modeled the Ne and Mg edges by fitting the X-ray spectrum in small wavelength intervals: the 8.5–10.5 Å region for Mg and the 13.0–16.0 Å region for Ne. We assumed that the spectrum in each of these intervals can be modeled with a power-law function ($F_\lambda \propto [\lambda/\lambda_{\text{edge}}]^\alpha$) and modeled each edge with a function of the form

$$F_\lambda = \begin{cases} F_\lambda & \text{for } \lambda > \lambda_{\text{edge}} \\ F_\lambda \exp \left[-A \left(\frac{\lambda}{\lambda_{\text{edge}}} \right)^3 \right] & \text{for } \lambda \leq \lambda_{\text{edge}}. \end{cases} \quad (1)$$

There are uncertainties in the positions of edges that are comparable to the resolution of the detector (Juett et al. 2004). Because of the relatively low signal-to-noise of the data, leaving the edge positions as free parameters did not affect the results of the fits. We, therefore, fixed the edge positions at the values inferred from high resolution X-ray

spectroscopy of X-ray binaries; i.e., $\lambda_{\text{edge}} = 9.5 \text{ \AA}$ for Mg (Ueda et al. 2005) and 14.3 \AA for Ne (Juett et al. 2004). We show the spectrum and the best fit models in Figure 1 and summarize the results of the fits in Table 2. Using the best-fit absorption coefficients and the cross-sections from Gould & Jung (1991), we then determined the column densities of each element. Our best fit values are $(9.65 \pm 1.56) \times 10^{17} \text{ cm}^{-2}$ for N_{Ne} and $(2.42 \pm 0.87) \times 10^{17} \text{ cm}^{-2}$ for N_{Mg} . Here and throughout this paper, the errors denote $1-\sigma$ uncertainties.

Using these values and assuming the ISM abundances reported by Wilms et al. (2000), we inferred a Galactic hydrogen column density towards 4U 1608–52 of $(1.08 \pm 0.16) \times 10^{22} \text{ cm}^{-2}$. We note here that the hydrogen column density inferred from an analysis of the continuum spectrum of 4U 1608–52 obtained from EXOSAT observations is $(1.0\text{--}1.5) \times 10^{22} \text{ cm}^{-2}$ (Penninx et al. 1989).

2.1. Conversion from Hydrogen Column Density to Infrared Extinction

Comparing the interstellar extinction determined from the X-ray grating spectrum with the K band extinction of red clump stars (see §3) requires converting the hydrogen column density to an infrared extinction A_K . We carry out this conversion in two steps using empirical laws that stem from observations of large samples of sources. We first convert from N_{H} to optical extinction A_V and subsequently from A_V to A_K .

The observed relation between hydrogen column density and optical extinction has been the subject of numerous studies (e.g., Görenstein 1975; Predehl & Schmitt 1996; Güver & Özel 2009). Using a variety of X-ray sources such as supernova remnants or X-ray binaries, the relation between N_{H} and A_V has been measured along different lines of sight. All of the studies found a relatively tight linear relationship between these quantities and none revealed any significant variation along different lines of sight.

Here, we use the relation

$$N_{\text{H}} = (2.21 \pm 0.09) \times 10^{21} \times A_V. \quad (2)$$

(see Güver & Özel 2009 and references therein) to convert the hydrogen column density to optical extinction. This result comes from the most recent effort to quantify the A_V – N_{H} relation and is based on high resolution spectra of 22 supernova remnants. The uncertainty in the normalization incorporates the uncertainties in the measurements of both quantities for each source and reflects also the variation along different lines of sight that is consistent with the data. This is why the uncertainty in the normalization is larger compared to previous studies despite the higher quality data used and the larger number of sources. Using this conversion law, we found an optical extinction towards the X-ray binary of $4.89 \pm 0.75 \text{ mag}$.

We carried out the second conversion between optical and infrared extinction following the empirical relation of Cardelli, Clayton, & Mathis (1989). Using a large sample of stars, these authors showed that *(i)* the extinction law is highly uniform for wavelengths greater than 0.7 microns (where the K band lies), *(ii)* the extinction law depends very weakly on R_V in this wavelength range, and *(iii)* it has extremely little scatter along different lines of sight. The ratio A_K/A_V is found empirically to depend on the parameter R_V according to the relation

$$\frac{A_K}{A_V} = 0.1615 - \frac{0.1483}{R_V}. \quad (3)$$

Allowing the parameter R_V^{-1} to take values in the range 0.2–0.4, as in the observed sample of Cardelli et al. (1989), we find that the ratio A_K/A_V ranges between 0.10–0.13. We assume a box-car distribution for the ratio A_K/A_V within this range. We found an extinction of $A_K = 0.56 \pm 0.11$ mag towards 4U 1608–52.

3. Determination of the Distance to 4U 1608–52 by Means of Red Clump Stars

In order to determine the distance to 4U 1608–52, we use a technique that relies on the red clump stars that are present in the field of view of the source. This method, discussed in detail in López-Corredoira et al. (2002) and Cabrera-Lavers, Garzón, & Hammersley (2005) is very reliable in deriving both the stellar number density and the interstellar extinction along a given line of sight in the Galaxy. Recently, a very similar method has been applied to determine the distances to some anomalous X-ray pulsars by Durant & van Kerkwijk (2006b).

Red clump giants have long been proposed as standard candles (Paczynski & Stanek 1998). These are core helium-burning giants with a very narrow luminosity function that constitute a compact and well-defined clump in an Hertzsprung-Russell (HR) diagram, particularly in the infrared. Furthermore, as they are relatively luminous, they can be identified to large distances from the Sun. The location of stars of the same spectral type (i.e., of approximately the same absolute magnitude) in a Color-Magnitude Diagram (CMD) depends on distance and extinction. The effect of distance alone shifts the stars to fainter magnitudes (vertically), while extinction by itself makes the stars both redder and fainter (shifting them diagonally in the CMD).

The absolute magnitude (M_K) and intrinsic color, $(J - K_s)_0$, of the red clump giants are well established (Alves 2000; Grocholski & Sarajedini 2002; Salaris & Girardi 2002; Pietrzyński et al. 2003). Here, we assume an absolute magnitude for the red clump popu-

lation of -1.62 ± 0.03 mag and an intrinsic color of $(J - K_s)_0 = 0.7$ mag. These values are consistent with the results derived by Alves (2000) from the *Hipparcos* red clump data and also with the results obtained by Grocholski & Sarajedini (2002) for open clusters. They are also in agreement with the intrinsic colors for the red clump stars predicted by the Padova isochrones in the 2 Micron All Sky Survey (2MASS) system (Bonatto et al. 2004) for a 10 Gyr population of solar metallicity of $(J - K)_0 = 0.68$ mag.

The absolute magnitudes of the red clump stars have a small dependence on metallicity (Salaris & Girardi 2002). For our case, this effect is negligible as there is no large metallicity gradient in the Galactic disc (Ibata & Gilmore 1995a, 1995b; Sarajedini, Lee, & Lee 1995). However, the red clump star absolute magnitude in the J band is more sensitive to metallicity and age than the K band, hence the intrinsic color $(J - K)_0$ also depends on both the metallicity and age (Salaris & Girardi 2002; Grocholski & Sarajedini 2002; Pietrzyński et al. 2003). For 4U 1608–52 ($l=331.0^\circ$, $b=-0.9^\circ$), in particular, the maximum metallicity gradient expected in this field produces a de-reddened color of $(J - K)_0 = 0.67 \pm 0.01$, considering the recent results in the metallicity for red clump giants in the inner Galaxy ($[\text{Fe}/\text{H}]=-0.2$ dex, González-Fernández et al. 2008), as well as the predictions of the theoretical isochrones of Salaris & Girardi (2002) and Bonatto et al. (2004) for this range of metallicities.

In summary, the metallicity dependence leads to a systematic uncertainty of 0.03 mag in the absolute magnitude of the red clump stars and to 0.05 mag in the intrinsic color $(J - K)_0$ (a value that also takes into account the dispersion around the mean color of the red clump population). We will adopt these values when determining the systematic uncertainties in the interstellar extinction along the line of sight to 4U 1608–52.

3.1. Application to the Case of 4U 1608–52

To apply the red clump method in the Galactic field we are interested in, we first build a $(J - K, K)$ CMD. In the case of 4U 1608–52, we use the data from 2MASS (Skrutskie et al. 2006) which is the most complete database of NIR Galactic point sources available to date. The 2MASS JHK photometry is slightly shallower than that provided by the more recent UKIDSS *Galactic Plane Survey* (Lucas et al. 2008). However, the latter survey has no coverage in the region where 4U 1608–52 lies, hence we rely on the 2MASS data only.

In order to isolate the red clump sources, we use the theoretical traces to define the limits of the K-giant branch on the CMDs (see Fig. 2). The traces are obtained for different stellar types by using a double exponential approximation to the interstellar extinction according to the updated “SKY” model (Wainscoat et al. 1992). This very simple approach is used

solely to facilitate the separation of the K-giant branch and has no effect on the final results. We then visually decide on the traces that are most useful in isolating the K-giants. Our goal is to avoid any kind of contamination in the red clump counts by other star populations, mainly dwarf stars and M-giants (see Fig. 2).

Once the optimal traces have been selected, we extract the giant stars from the CMD and bin them according to their K magnitudes. For each magnitude bin, we construct count histograms by making horizontal cuts (i.e., running color) through the CMDs at each range of K magnitudes. We then fit a Gaussian function

$$f(x; A, \mu, \sigma) = A \exp \left[-\frac{(x - \mu)^2}{2\sigma^2} \right], \quad (4)$$

where x is the binned ($J - K$) color and μ is the color of the peak, to the histogram to determine the position of the peak in each cut.

Figure 3 shows different Gaussian fits to the color histograms obtained in three different magnitude bins for the field of Figure 2. The identified maxima correspond to the red clump stars since they are by far the most prominent population (Hammersley et al. 2000; Cohen et al. 2000).

The fits provide simultaneously the magnitude m_K and the color $J - K$ for each maximum. We use these fits to determine the extinction $A_K(m_K)$ by tracing how the $J - K$ colors of the peaks of the red clump counts change with m_K . We calculate the extinction for any given m_K using the measured ($J - K$) of the peak, the intrinsic mean color excess definition, and the interstellar extinction values for A_J and A_K , i.e.

$$A_K = c_e \times [(J - K)_{m_K} - (J - K)_0], \quad (5)$$

where $c_e=0.657$ (Rieke & Lebofsky 1985; this value is consistent with the one found by Cardelli et al. 1989). We then obtain the extinction $A_K(r)$ to a heliocentric distance r for each field by using the usual transformation for the distance along the line of sight:

$$r = 10^{[m_K - M_K + 5 - A_K(r)/5]}. \quad (6)$$

We estimate the uncertainties in the extinction from the uncertainty of the mean color of the Gaussian component

$$\sigma_{JKm} = \frac{\sigma}{1.52\sqrt{N}}, \quad (7)$$

where $N = A\sigma\sqrt{2\pi}$ is the total number of red clump stars in each magnitude bin. This uncertainty gives an indicator of the statistical error only; to determine the total uncertainty in the extinction, we also take into account the spread $\sigma_{JK0}=0.05$ mag in the intrinsic color, $(J - K)_0$, of the red clump population due to metallicity effects and add both uncertainties in quadrature:

$$\sigma_{A_K}^2 = \sigma_{JKm}^2 + \sigma_{JK0}^2 \quad (8)$$

We calculate the uncertainty in the distance along the line of sight by means of equation (6) from: (i) the dispersion in the absolute magnitude of the red clump population, (ii) the uncertainties in the extinction given by equation (8), and (iii) the size of the binning in m_K used to perform the Gaussian fit of equation (4).

The only restriction that has to be taken into account when applying this method is the contamination in the red clump counts due to dwarf stars, which is important at $m_K > 13$ for in-plane fields (López-Corredoira et al. 2002). This imposes a limit in the distance along the line of sight up to which we can extract the interstellar extinction. For the field around 4U 1608–52, this value is nearly 7.5 kpc, which turns out to be larger than the inferred distance to the source.

3.2. The Distance to 4U 1608–52

From the 2MASS archival data, we have extracted stars in the field of view of 4U 1608–52, using an interval of $\Delta l=0.5^\circ$ and $\Delta b=0.3^\circ$, that gives a total number of 13202 stars. With those stars, we measured the run of reddening with distance up to ~ 7.5 kpc.

In principle, we can increase the accuracy in the determination of the extinction by enlarging the size of the region around the location of 4U 1608–52. This would increase the number of red clump stars, thus decreasing the uncertainty given by equation (7). At the same time, it would allow a decrease in the bin size in magnitude m_K that is used to perform the Gaussian fit of equation (4), yielding a better sampling of the extinction and a higher accuracy when deriving the distance.

To do this, however, we must first ensure that there are no significant variations in extinction in the lines of sight around 4U 1608–52. For this purpose, we collected 2MASS

data in two adjacent fields to 4U 1608–52, each 0.5 degrees away in longitude to the source (we will refer to them as ‘field A’ and ‘field B’). We find that there is no strong variation of extinction in those fields with respect to the values obtained for the field centered on 4U 1608–52 (see Fig. 4).

We merged all the data for the field centered on 4U 1608–52, using an interval for the extraction of 2MASS sources of $\Delta l=1.5^\circ$ and $\Delta b=0.3^\circ$, hence covering an area of $\sim 0.45 \text{ deg}^2$ in the sky. The resulting total number of stars increased to 40548 and the uncertainties in the extinction estimates decreased by a factor of 2.5. We show in Figure 5 the resulting CMD with the location for the maxima of the red clump population derived following our method. In Figure 6, we plot the inferred variation of extinction along the line of sight to 4U 1608–52.

To measure the distance to the binary, we compared the run of extinction using the red clump stars to that obtained from the X-ray spectrum of 4U 1608–52. We denote the probability distribution over extinction for the X-ray source as $P_X(A_K)$ and the one obtained for the red clump stars for each distance bin as $P_{RC}(A_K|D)$ and represent them by Gaussian functions. Because there are no priors on either the extinction or the distance,

$$P_{RC}(A_K|D) = P_{RC}(D|A_K). \quad (9)$$

We then calculated the total probability distribution by taking the product of these two independent probability distributions and marginalizing over the extinction:

$$P(D) = \int P_X(A_K) P_{RC}(D|A_K) dA_K. \quad (10)$$

In Figure 7, we show the probability distribution over distance calculated in this way. In order to find the distance with the highest probability, we then fit the distribution with a Gaussian function. Because there is a clear and sudden decrease in the extinction below 3.9 kpc, we added a cut-off to the Gaussian function below this distance. The best fit position of the Gaussian is $5.8^{+2.0}_{-1.8}$ kpc, where the positive uncertainty reflects the standard deviation of the Gaussian while the negative uncertainty corresponds to the low-end cutoff.

4. Modeling Type-I X-ray Bursts

We analyzed Rossi X-ray Timing Explorer (RXTE) Proportional Counter Array (PCA) archival observations of 4U 1608–52, which totaled 1650 ks of observing time until June 2007. We identified thermonuclear (Type-I) X-ray bursts in the archival data using the X-ray burst catalog of Galloway et al. (2008a). In total, we found 31 Type-I X-ray bursts from this source.

Using the *seextract* tool, we extracted 2.5–15.0 keV X-ray spectra from all of the RXTE/PCA layers. Following the analysis in Özel et al. (2009), we used either the Science Event mode data with the E_125 μ s_64M_0_1s configuration, which has a nominal time resolution of 125 μ s in 64 spectral channels, or we used *Good Xenon* mode data which has 0.95 μ s time resolution in 256 spectral channels, where available. We extracted spectra for 0.25, 0.5, 1, or 2 s time intervals, depending on the source count rate during the burst. However, due to some data gaps during the observations, in a few cases we had to use X-ray spectra integrated over smaller exposure times. As in Galloway et al. (2008a) and Özel et al. (2009), we also used a 16 s spectrum prior to the burst as background. We created separate response matrix files for each burst using the PCARSP version 10.1.

We used XSPEC v12.4.0 (Arnaud 1996) for spectral analysis. We fit the spectra with a blackbody function (bbodyrad model in XSPEC), fixing the hydrogen column density to the value found from the analysis of the high resolution grating spectra (see Section 2). We calculated the bolometric X-ray fluxes using the equation (3) of Galloway et al. (2008a). All errors correspond to 1- σ confidence levels of our fits.

We identified the photospheric radius expansion bursts in this sample by looking for (i) a clear difference in the apparent radius between the first seconds of the burst and during the cooling tail and (ii) a characteristic temperature evolution seen in PRE bursts. The spectral evolution of an example of these bursts is given in Figure 8. We found a total of five such bursts, in contrast to the 12 PRE bursts identified in Galloway et al. (2008a). The difference arises from the fact that the latter study categorized as PRE a number of bursts where the maximum radii reached during bursts does not differ significantly from the radii during the cooling tails. We show in Figure 9 an example of such a case. We did not classify these as PRE bursts and, thus, did not take them into account when determining the Eddington flux.

We used the PRE burst sample shown in Table 3 to measure the touchdown fluxes. We define the touchdown flux as the bolometric flux measured when the normalization of the blackbody gets its lowest and the temperature attains its highest value. In these bursts, the peak flux during the burst and the touchdown flux are consistent with each other to $\sim 5\%$ (c.f., Galloway, Özel, & Psaltis 2008b). Table 3 shows the measured touchdown fluxes. Although two other bursts (with IDs 4 and 5) showed clear evidence for a PRE event, data gaps during the touchdown instant prevented us from determining and using their touchdown flux values. We show in Fig. 10) the confidence contours for the color temperature and the normalization for the two PRE bursts during touchdown. We found a combined best fit value of $(1.541 \pm 0.065) \times 10^{-7}$ erg cm $^{-2}$ s $^{-1}$ for 4U 1608–52 for the touchdown flux.

The last spectroscopic quantity that we measured is the normalization of the blackbody

during the cooling tails of the bursts. This quantity is related to the apparent blackbody radius and the distance through $A = (R_{\text{app}}/D_{10 \text{ kpc}})^2$, where R is the apparent radius in km and the $D_{10 \text{ kpc}}$ is the distance in units of 10 kpc. During the cooling tails of the Type-I X-ray bursts, the blackbody radius attains a constant value, while the flux and the temperature decrease. In order to find an average normalization for each burst, we took the measurements in the 3–10 s time interval after each burst started, when the apparent radius reaches a constant value, while the signal-to-noise ratio remains high. We present in Table 4 the blackbody normalizations for the four bursts that showed this clear trend. Three out of the four measurements of the blackbody normalization are within $1-\sigma$, while the fourth measurement is within $2-\sigma$ of the rest. This implies that all measurements are consistent with each other within their formal uncertainties. Formally fitting these four values with a constant results in a blackbody normalization of $324.6 \pm 2.4 \text{ (km/10 kpc)}^2$.

5. Measurement of the Neutron Star Mass and Radius

The distance measurement to 4U 1608–52, the touchdown flux, and the blackbody normalization obtained by time resolved X-ray spectroscopy of the bursts provide the three observables that are needed to measure independently the mass and the radius of the neutron star in this binary. The observed spectral parameters depend on the stellar mass and radius according to the equations (Özel et al. 2009)

$$F_{TD} = \frac{GMc}{\kappa_{es}D^2} \left(1 - \frac{2GM}{Rc^2}\right)^{1/2} \quad (11)$$

and

$$A = \frac{R^2}{D^2 f_c^4} \left(1 - \frac{2GM}{Rc^2}\right)^{-1}, \quad (12)$$

where G is the gravitational constant, c is the speed of light, κ_{es} is the opacity to electron scattering, and f_c is the color correction factor. We use the electron scattering opacity $\kappa_{es} = 0.20(1 + X) \text{ cm}^2 \text{ g}^{-1}$, which depends on the hydrogen mass fraction X .

We assign independent probability distribution functions to the distance $P(D)dD$, the touchdown flux $P(F_{TD})dF_{TD}$ and the normalization $P(A)dA$ measurements, as well as to the possible range of the hydrogen mass fraction $P(X)dX$ and the color correction factor $P(f_c)df_c$. We then find the total probability density over the neutron star mass M and radius R by integrating the equation

$$P(D, X, f_c, M, R)dDdXd f_c dM dR = \frac{1}{2}P(D)P(X)P(f_c)P[F_{TD}(M, R, D, X)] \\ \times P[A(M, R, D, f_c)]J\left(\frac{F_{TD}, A}{M, R}\right)dDdXd f_c dM dR, \quad (13)$$

over the distance, the hydrogen mass fraction, and the color correction factor. Here, $J(F_{TD}, A|M, R)$ is the Jacobian of the transformation from the variables (F_{TD}, A) to (M, R) .

In the absence of any observable constraints on the hydrogen mass fraction, we assign a box-car probability distribution, allowing it to cover the range from 0.0 to 0.7, i.e.,

$$P(X)dX = \begin{cases} \frac{1}{\Delta X} & \text{if } |X - X_0| \leq \Delta X/2 \\ 0 & \text{otherwise} . \end{cases} \quad (14)$$

with $X_0 = 0.35$ and $\Delta X = 0.7$.

For the color correction factor f_c , we take a box-car probability distribution covering the range 1.3 – 1.4, so that

$$P(f_c)d f_c = \begin{cases} \frac{1}{\Delta f_c} & \text{if } |f_c - f_{c0}| \leq \Delta f_c/2 \\ 0 & \text{otherwise} , \end{cases} \quad (15)$$

where $f_{c0} = 1.35$ and $\Delta f_c = 0.1$. This is motivated by model atmosphere calculations shown in Figure 11 for a range of neutron star surface gravity strengths and metallicities that are consistent with the absence of atomic lines in the high resolution X-ray spectra of bursters (see Madej, Joss & Różańska 2004 and Psaltis & Özel 2009 for the details of the calculations). The models of Majczyna et al. (2005) with solar and higher iron abundances have significant line features that have not been detected in any high resolution burst spectra; nevertheless, they result in very similar values of the color correction factor. Because the color correction is applied to the temperature measured during the cooling tails of bursts, where the flux has dropped to less than half the Eddington flux (for a given surface gravity), the relevant range of values is indicated with dashed lines, which corresponds to the distribution quoted above.

All of the three measurements we use here are dominated by statistical errors. For the distance, we use the parameters of the Gaussian presented in Section 3, with a cutoff in the probability distribution function below 3.9 kpc,

$$P(D)dD = \begin{cases} 0 & \text{for } D < 3.9 \text{ kpc} \\ \exp[-\frac{(D-D_0)^2}{2\sigma_D^2}] & \text{for } D > 3.9 \text{ kpc.} \end{cases} \quad (16)$$

appropriately normalized.

Similarly, we assign a Gaussian probability distribution to the blackbody normalization obtained from the bursts,

$$P(A)dA = \frac{1}{\sqrt{2\pi\sigma_A^2}} \exp[-\frac{(A-A_0)^2}{2\sigma_A^2}] \quad (17)$$

with $A_0 = 324.6$, $\sigma_A = 2.4$ (km/10 kpc)².

For the touchdown flux, we take a Gaussian probability distribution and use the best fit value and its standard deviation given in Section 4.

$$P(F_{TD})dF_{TD} = \frac{1}{\sqrt{2\pi\sigma_F^2}} \exp[-\frac{(F_{TD}-F_0)^2}{2\sigma_F^2}] \quad (18)$$

The final distribution over the neutron star mass and radius is obtained by inserting each probability distribution into equation (13) and integrating over the distance and the hydrogen mass fraction. Figure 12 shows the 1 and 2 $-\sigma$ contours for the mass and the radius of the neutron star in 4U 1608–52.

6. Discussion

In this paper, we combined a distance measurement technique, applied for the first time to a LMXB, with time resolved spectroscopy of the Type-I X-ray bursts in order to measure the mass and the radius of the neutron star in the X-ray binary 4U 1608–52. There are no previous distance measurements to this binary. Our analysis led to a distance of 5.6 ± 1.5 kpc, which, together with the galactic coordinates of the source, implies that 4U 1608–52 is either on the far side of the Scutum-Crux arm or in between the Scutum-Crux and Norma arms. Between these two galactic arms, the increase in the extinction is expected to be minor. Our analysis of the run of reddening with extinction using the red clump giants along this line

of sight showed this expected trend. Because 4U 1608–52 falls in a region between the arms where the slope of the extinction curve shown in Figure 6 is very shallow, the errors in the distance measurement, correspondingly, are relatively large. Nevertheless, a firm lower limit is achieved on the source distance.

The 1- and 2- σ confidence contours of mass and radius shown in see Figure 12 are based on the distance measurement and spectral analysis of the X-ray bursts observed from this source. We also find the individual probability density functions for mass and radius by marginalizing $P(M, R)$ over radius and mass, respectively. Fitting the resulting probability distributions with Gaussian functions yields a mass of $M = 1.74 \pm 0.14 M_{\odot}$ and a radius of $R = 9.3 \pm 1.0$ km, where the errors represent 1- σ uncertainties.

There are numerous mass measurements and estimates of isolated and binary neutron stars. Dynamical mass measurements allow, in some cases, very precise determination of the neutron star masses (see Thorsett & Chakrabarty 1999 for a review). However, dynamical measurements do not reveal any information about the neutron star radii, which are better indicators of the neutron star equation of state than are masses (Özel & Psaltis 2009).

Most attempts at measuring neutron star radii result in constraints on the *combination* of neutron star radii and masses. Such measurements have been carried out on globular cluster neutron stars in binaries emitting thermally during quiescence, such as X7 in 47 Tuc and others in ω Cen, M 13, and NGC 2808 (Heinke et al. 2006; Webb & Barret 2007). These measurements have carved out large allowed bands in the mass-radius plane, covering the mass-radius contours of the present measurements.

Using multiple spectroscopic phenomena, on the other hand, leads to an independent measurement of the stellar radius and mass. Özel (2006) used spectroscopic measurements of the Eddington limit and apparent surface area during thermonuclear bursts, in conjunction with the detection of a redshifted atomic line from the source EXO 0748–676, to determine a mass of $M \geq 2.10 \pm 0.28 M_{\odot}$ and a radius $R \geq 13.8 \pm 1.8$ km. Özel et al (2009) applied an approach similar to the one in the current paper to a neutron star binary EXO 1745–248 in the globular cluster Terzan 5 and found tightly constrained pairs of values for the mass and radius, which are centered around $M = 1.4 M_{\odot}$ and $R = 11$ km or around $M = 1.7 M_{\odot}$ and $R = 9$ km. The latter two radius measurements are consistent with the one presented in the current paper to within 2- σ , and, therefore, several nucleonic equations of state are consistent with both measurements.

The systematic and statistical errors on the measured masses and radii of neutron stars do not yet allow the determination of a unique equation of state for neutron star matter. However, by measuring a sufficient number of neutron stars with different masses, it is

possible to trace out the mass and radius relation, which would then allow a measurement of the pressure of cold ultradense matter at densities beyond the nuclear saturation density (Özel & Psaltis 2009). In the present calculations, the largest uncertainty arises from the distance measurement, due both to the particular location of the binary in the Galactic disk as well as to the short exposure time of the X-ray grating observation that yields a low signal-to-noise spectrum. Future X-ray grating observations will help decrease the distance uncertainty and improve the mass and the radius measurement as well.

We thank D. Psaltis and S. Bilir for very useful discussions and an anonymous referee for numerous constructive suggestions that improved the analysis. F. Ö. acknowledges support from NSF grant AST 07-08640. This work made use of observations obtained with XMM-Newton, an ESA science mission with instruments and contributions directly funded by ESA Member States and NASA. This publication also made use of data products from the Two Micron All Sky Survey, which is a joint project of the University of Massachusetts and the Infrared Processing and Analysis Center/California Institute of Technology, funded by the National Aeronautics and Space Administration and the National Science Foundation.

REFERENCES

- Alves, D. R. 2000, *ApJ*, 539, 732
- Arnaud, K. A. 1996, in *ASP Conf. Series*, Vol. 101, ADASS V, ed. G. H. Jacoby & J. Barnes, 17
- Belian, R. D., Conner, J. P., & Evans, W. D. 1976, *ApJ*, 206, L135
- Bildsten, L. 1998, in *NATO ASI Proc. C515: The Many Faces of Neutron Stars.*, ed. R. Bucheri, J. van Paradijs, & A. Alpar, 419
- Bonatto, C., Bica, E., & Girardi, L. 2004, *A&A*, 415, 571
- Cabrera-Lavers, A., Garzón, F., & Hammersley, P. L. 2005, *A&A*, 433, 173
- Cardelli, J. A., Clayton, G. C., & Mathis, J. S. 1989, *ApJ*, 345, 245
- Cohen, M., Hammersley, P. L., & Egan, M. P. 2000, *AJ*, 120, 3362
- Durant, M., & van Kerkwijk, M. 2006a, *ApJ*, 650, 1070
- 2006b, *ApJ*, 650, 1082

- Freeman, P., Doe, S., & Siemiginowska, A. 2001, *Proc. SPIE*, 4477, 76
- Fujimoto, M. Y., Hanawa, T., & Miyaji, S. 1981, *ApJ*, 247, 267
- Galloway, D., Muno, M., Hartman, J., Savov, P., Psaltis, D., & Chakrabarty, D. 2008a, *ApJS*, 179, 360
- Galloway, D., Özel, F., & Psaltis, D. 2008b, *MNRAS*, 387, 268
- González-Fernández, C., Cabrera-Lavers, A., Hammersley, P. L., & Garzón, F. 2008, *A&A*, 479, 131
- Gould, R. J., & Jung, Y. D. 1991, *ApJ*, 373, 271
- Grocholski, A. J., & Sarajedini, A. 2002, *AJ*, 123, 1603
- Görenstein, P. 1975, *ApJ*, 198, 95
- Grindlay, J. E., & Liller, W. 1978, *ApJ*, 220, L127
- Güver, T., Özel, F. 2009, *MNRAS*, 400, 2050
- Hammersley, P. L., Garzón, F., Mahoney, T. J., López-Corredoira, M., & Torres, M. A. P. 2000, *MNRAS*, 317, L45
- Heinke, C. O., Rybicki, G. B., Narayan, R., & Grindlay, J. E. 2006, *ApJ*, 644, 1090
- Ibata, R. A., & Gilmore, G. F. 1995a, *MNRAS*, 275, 591
- 1995b, *MNRAS*, 275, 605
- Juett, A., Schulz, N., & Chakrabarty, D. 2004, *ApJ*, 612, 308
- Juett, A. M., Schulz, N. S., Chakrabarty, D., & Gorczyca, T. W. 2006, *ApJ*, 648, 1066
- Lattimer, J., & Prakash, M. 2001, *ApJ*, 550, 426
- 2007, *Phys.Rep.*, 442, 109
- Lewin, W. H. G., van Paradijs, J., & Taam, R. E. 1993, *Space Science Reviews*, 62, 223
- López-Corredoira, M., Cabrera-Lavers, A., Garzón, F., & Hammersley, P. L. 2002, *A&A*, 394, 883
- Lucas, P. W. et al. 2008, *MNRAS in press*, arXiv:0712.0100

- Madej, J., Joss, P. C., & Różańska, A. 2004, *ApJ*, 602, 904
- Majczyna, A., Madej, J., Joss, P. C., & Różańska, A. 2005, *A&A*, 430, 643
- Özel, F. 2006, *Nature*, 441, 1115
- Özel, F., Güver, T., & Psaltis, D. 2009, *ApJ*, 693, 1775
- Özel, F. & Psaltis, D. 2009, *Phys. Rev. D*, 80, 103003
- Paczynski, B., & Stanek, K. Z. 1998, *ApJ*, 494, L219
- Penninx, W., Damen, E., van Paradijs, J., Tan, J., & Lewin, W. H. G. 1989, *A&A*, 208, 146
- Pietrzyński, G., Gieren, W., & Udalski, A. 2003, *AJ*, 125, 2494
- Psaltis, D. & Özel, F. 2009, in preparation
- Rieke, G. H., & Lebofsky, M. J. 1985, *ApJ*, 288, 618
- Salaris, M., & Girardi, L. 2002, *MNRAS*, 337, 332
- Sarajedini, A., Lee, Y. W., & Lee, D. H. 1995, *ApJ*, 450, 712
- Skrutskie, M. F. et al. 2006, *AJ*, 131, 1163
- Tananbaum, H., Chaisson, L. J., Forman, W., Jones, C., & Matilsky, T. A. 1976, *ApJ*, 209, L125
- Thorsett, S. E. & Chakrabarty, D. 1999, *ApJ*, 512, 288
- van Paradijs, J. 1978, *Nature*, 274, 650
- van Paradijs, J. 1979, *ApJ*, 234, 609
- van Paradijs, J. & White, N. 1995, *ApJ*, 447, 33
- Wachter, S., Hoard, D. W., Bailyn, C. D., Corbel, S., & Kaaret, P. 2002, *ApJ*, 568, 901
- Wainscoat, R. J., Cohen, M., Volk, K., Walker, H. J., & Schwartz, D. E. 1992, *ApJS*, 83, 111
- Webb, N. A., & Barret, D. 2007, *ApJ*, 671, 727
- Wilms, J., Allen, A., & McCray, R. 2000, *ApJ*, 542, 914
- Wroblewski, P., Güver, T., & Özel, F. 2008, arXiv:0810.0007v1 [astro-ph]

Table 1. Log of all the XMM-Newton observations of 4U 1608–52.

Date	Obs. ID	Exp. Time (ks)
2002-02-13	0074140301	2.9
2002-02-13	0074140101	17.2
2002-02-15	0074140201	16.9
2003-03-14	0149180201	7.2

Table 2. Best fit values of the parameters for the model

Element	Γ	Ampl. (10^{-2})	Abs. Coef.	N (10^{17} cm^{-2})	N_{H} (10^{22} cm^{-2})	$\chi^2/\text{d.o.f.}$
Mg	3.80 ± 0.06	1.34 ± 0.02	0.053 ± 0.019	2.42 ± 0.87	0.96 ± 0.34	1.1 (114 d.o.f.)
Ne	7.69 ± 0.35	0.85 ± 0.02	0.34 ± 0.06	9.65 ± 1.56	1.11 ± 0.18	1.4 (114 d.o.f.)

Table 3. Properties of the PRE bursts used to find the unabsorbed touchdown flux. Burst start times are adopted from Galloway et al. (2008a).

ID	Obs ID.	MJD	Touchdown Flux ($10^{-7} \text{ erg cm}^{-2} \text{ s}^{-1}$)
1	30062-01-01-00	50899.58703	1.558 ± 0.082
2	70059-03-01-000	52529.17934	1.514 ± 0.105

Table 4. Properties of the bursts used to find the normalization value during the cooling tail. Burst start times are adopted from Galloway et al. (2008a).

ID	Obs ID.	MJD	Normalization ($R_{\text{km}}/D_{10\text{kpc}})^2$
2	70059-03-01-000	52529.17934	326.7 ± 4.7
3	10093-01-03-000	50164.69334	330.2 ± 4.9
4	70059-01-20-00	52524.10157	325.8 ± 5.4
5	70059-01-21-00	52526.16006	317.0 ± 4.5

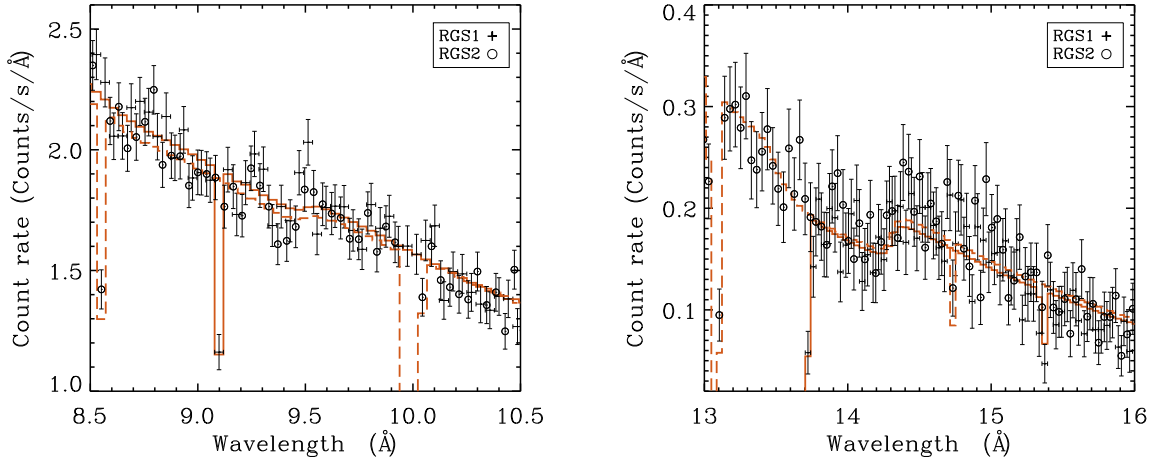


Fig. 1.— RGS1 and RGS2 spectra of 4U 1608–52 together with the best fit models (solid line for RGS1 and dashed line for RGS2) are given for the regions that are used to determine the column densities of Mg (left panel) and Ne (right panel). Sharp features are due to CCD gaps and the malfunctioning CCD in the RGS detector.

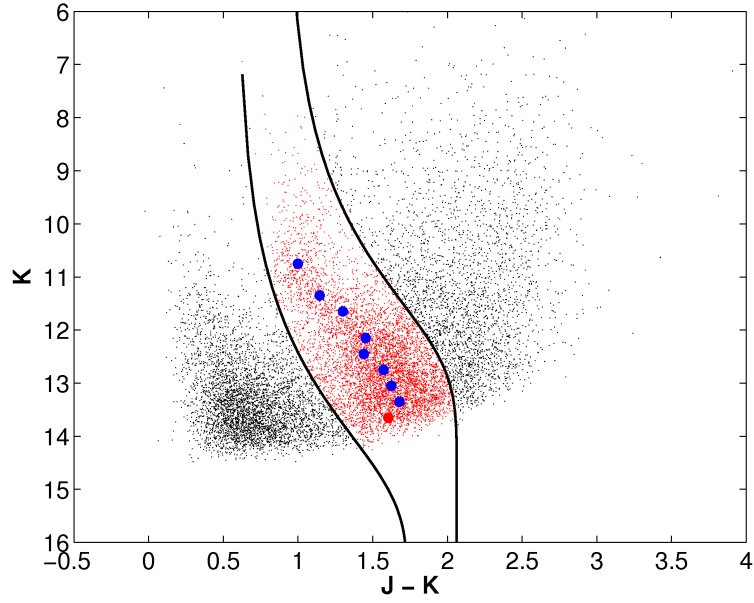


Fig. 2.— NIR color-magnitude diagram for a 0.15 deg^2 field centered around 4U 1608–52 ($l = 330.9^\circ$ $b = -0.9^\circ$) and, taken from the 2MASS survey. The solid lines delimit the region where the red clump giants lie. Filled circles show points of maximum density of red clump stars for each individual magnitude bin.

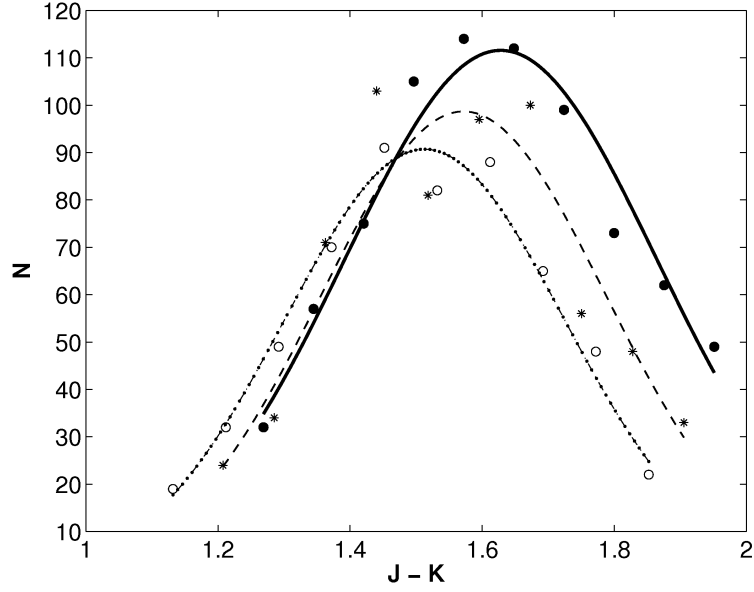


Fig. 3.— Gaussian fits (lines) to the red clump counts (points) in three magnitude bins for the 0.15 deg^2 field around 4U 1608–52. The solid line (filled circles) corresponds to the $12.6 < m_K < 12.9$ bin, the dashed line (asterisks) to the $12.3 < m_K < 12.6$ bin, and the dot-dashed line (open circles) to the $12.0 < m_K < 12.3$ bin.

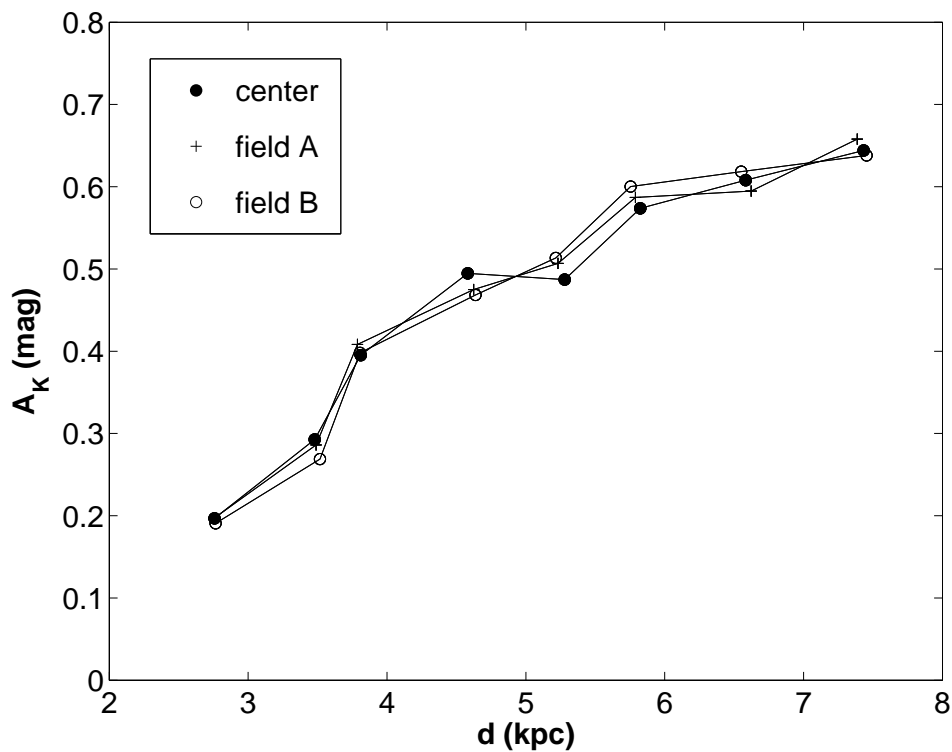


Fig. 4.— K-band extinctions along the line of sight for the field 1.5 deg^2 centered around 4U 1608–52 (filled circles), and for two adjacent fields 0.5 deg away in longitude, labelled as 'field A' (pluses) and 'field B' (open circles). As it can be seen, there are no significant variations between three fields.

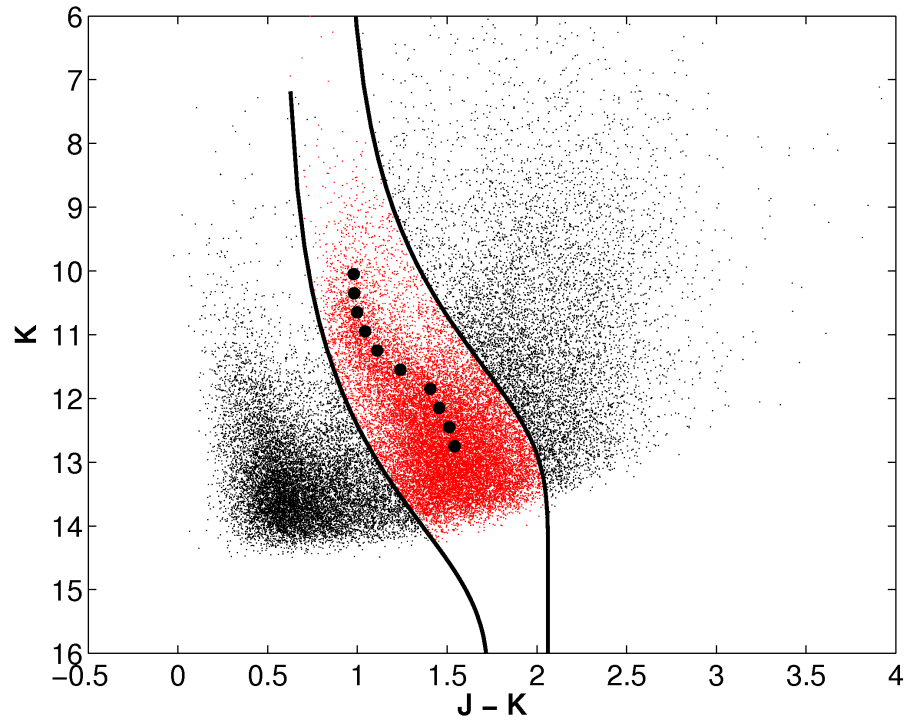


Fig. 5.— Same as Fig. 2, but now considering a 0.45 deg^2 field centered around 4U 1608–52 ($l = 330.9^\circ$ $b = -0.9^\circ$).

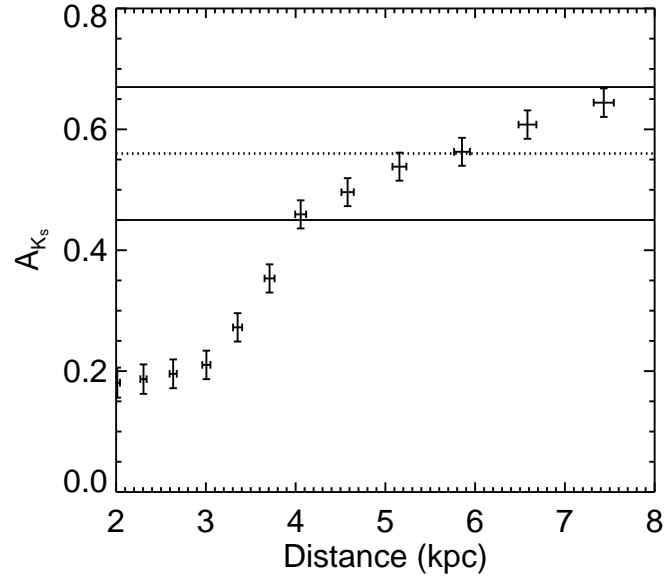


Fig. 6.— The K-band extinction curve along the line of sight to 4U 1608–52 using a 0.45 deg^2 field surrounding it. Overplotted are the A_K value for 4U 1608–52 and its $1-\sigma$ statistical error.

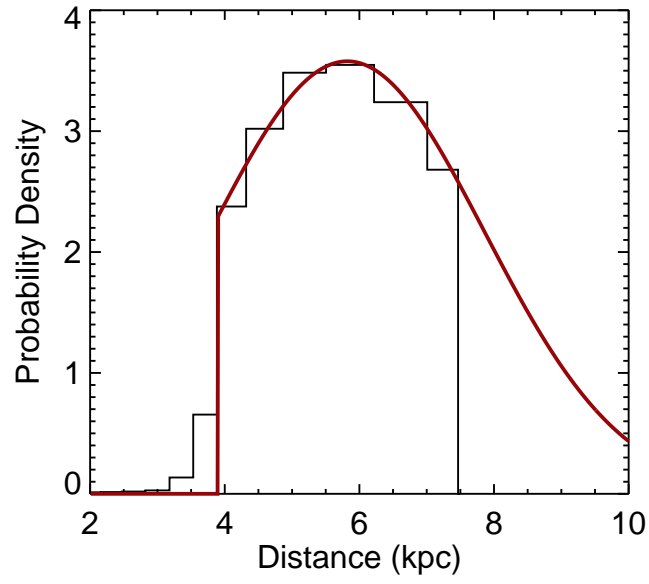


Fig. 7.— The probability distribution over distance to the source 4U 1608–52 and the best fit Gaussian model with a cut-off at 3.9 kpc. The best fit distance is found to be 5.42 ± 1.00 kpc.

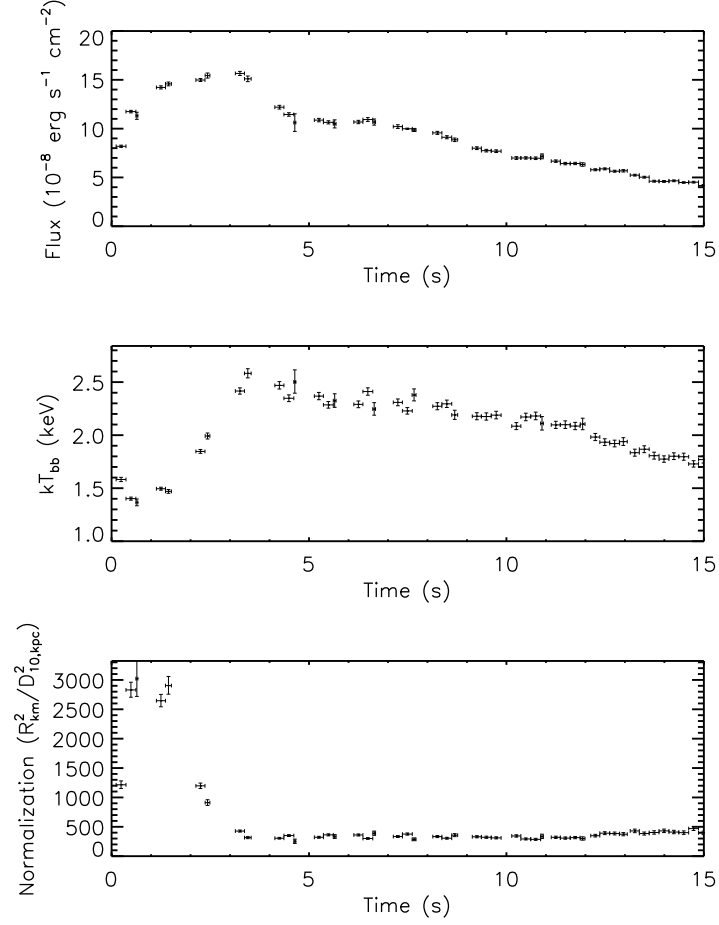


Fig. 8.— Spectral evolution during the first fifteen seconds of one the Eddington limited thermonuclear X-ray bursts (ID 70059-03-01-000). The three panels show the flux, black-body temperature and the normalization values together with their $1-\sigma$ statistical errors, respectively.

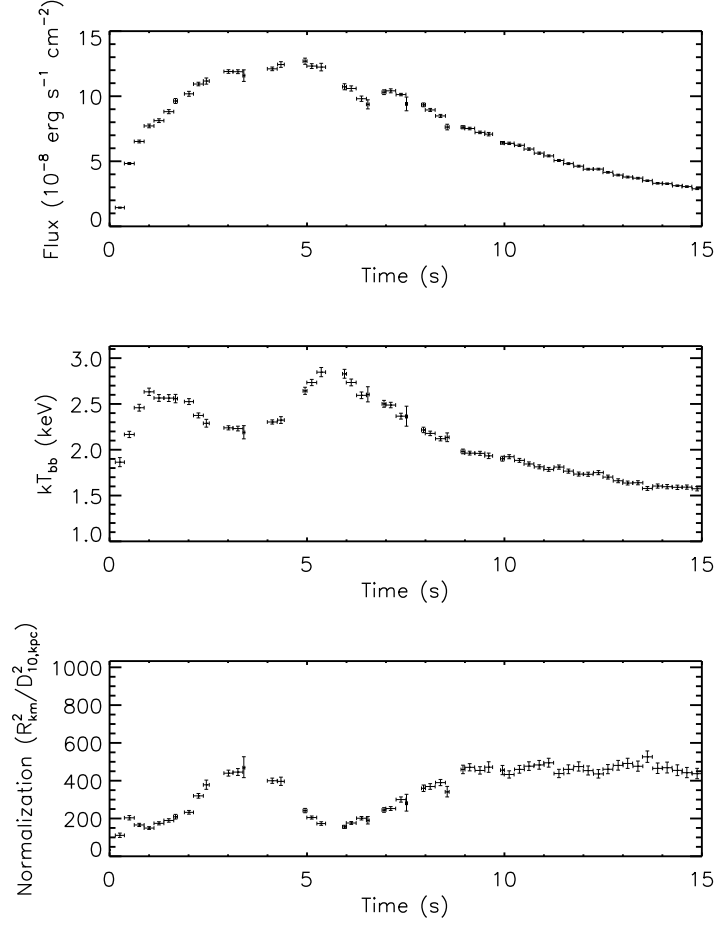


Fig. 9.— Same as Figure 8, but for an X-ray burst (ID 70059-01-26-00) that had previously been categorized as PRE (Galloway et al. 2008a) but did not meet our PRE identification criteria. Such bursts were not used in the analysis.

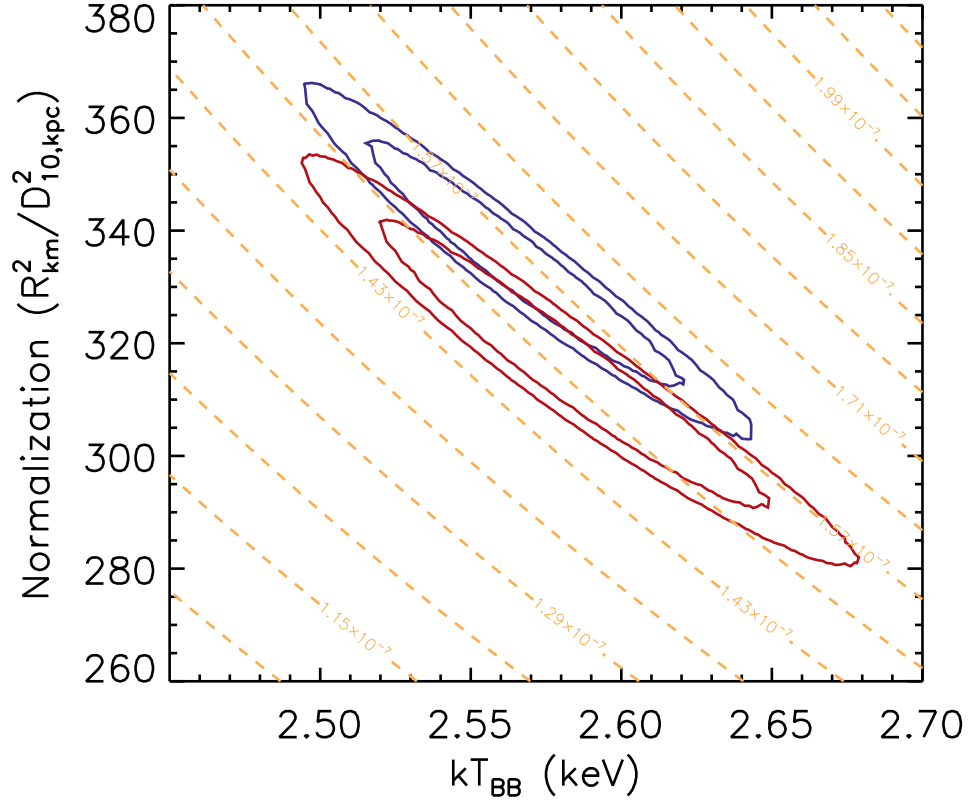


Fig. 10.— The 1- and 2- σ confidence contours of the normalization and the blackbody temperature obtained from fitting the two PRE bursts during touchdown. The dashed lines show contours of constant bolometric flux.

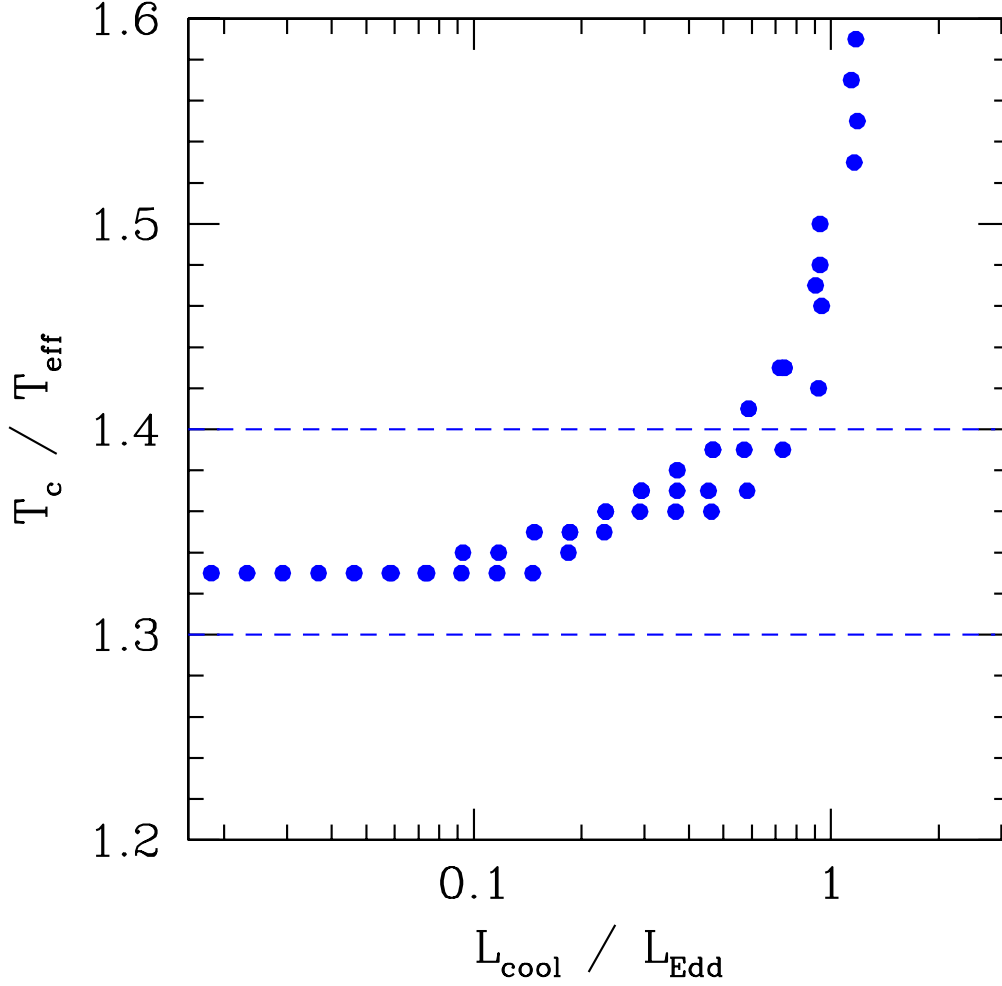


Fig. 11.— The color correction factor $f_c = T_c/T_{\text{eff}}$ against the surface luminosity normalized to the Eddington luminosity. The values are obtained from model atmosphere calculations for a range of surface gravity strengths and for small metallicities that are consistent with the absence of atomic lines in the high resolution X-ray spectra of bursters. The dashed lines indicate the range of color correction factors taken in the present work for the calculation of the apparent area of the neutron star during the cooling tails of bursts, where the luminosity drops to values less than $0.5L_{\text{Edd}}$.

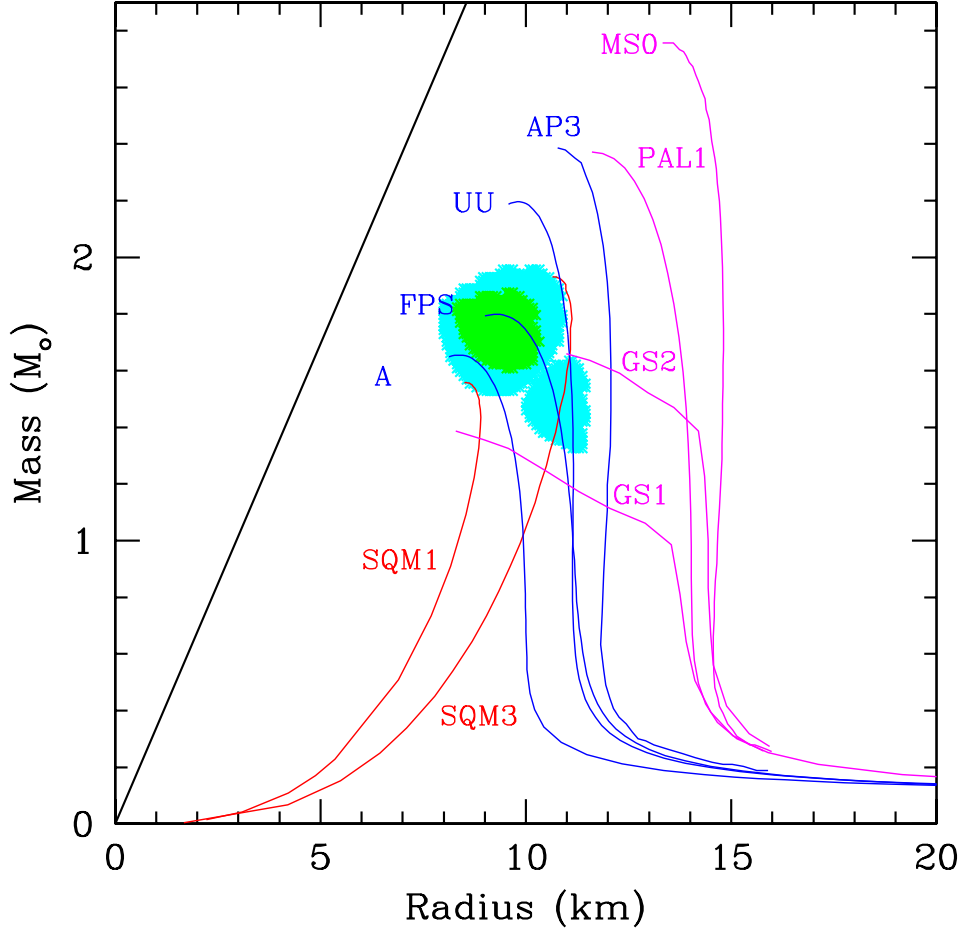


Fig. 12.— The 1- and 2- σ contours for the mass and the radius of the neutron star in 4U 1608–52. The descriptions of the various equations of state and the corresponding labels can be found in Lattimer & Prakash (2001).